Reorganization of human cortical maps caused by inherited photoreceptor abnormalities

Heidi A. Baseler[1], Alyssa A. Brewer[2], Lindsay T. Sharpe[3], Antony B. Morland[1], Herbert Jägle[3] and Brian A. Wandell[1,2]

[1] *Department of Psychology,* [2]*Neuroscience Program, Stanford University, Stanford, California, USA*

[3] *University of Tübingen, Tübingen, Germany*

Correspondence should be addressed to B.A.W. (wandell@stanford.edu)

Published online: 25 February 2002, DOI: 10.1038/nn817

We describe a compelling demonstration of large-scale developmental reorganization in the human visual pathways. The developmental reorganization was observed in rod monochromats, a rare group of congenitally colorblind individuals who virtually lack cone photoreceptor function. Normal controls had a cortical region, spanning several square centimeters, that responded to signals initiated in the all-cone foveola but was inactive under rod viewing conditions; in rod monochromats this cortical region responded powerfully to rod-initiated signals. The measurements trace a causal pathway that begins with a genetic anomaly that directly influences sensory cells and ultimately results in a substantial central reorganization.

The normal human retina contains a small rod-free zone, the foveola. This zone spans a diameter of 1.25 deg of visual angle[1–4]. The signals initiated by the cones in the foveola are represented over a disproportionately large area of visual cortex: while the foveola occupies <1% of the retina, the cortical representation of the foveola occupies roughly 20% of primary visual cortex (V1)[5,6]. Moreover, because of the confluence of the foveolar representations in areas V1, V2 and V3, the combined pure-cone region occupies roughly 4–5 cm^2 near the occipital pole.

Rod monochromats, who lack most or all input from cones, provide a unique opportunity to examine how human visual cortex reorganizes in response to abnormal visual experience. Their genetic defects cause a malfunction in the phototransduction cascade in all three types of cone photoreceptors[7–9]. There is no evidence of any genetic abnormalities in monochromats that could directly alter cortical structure, or even post-receptoral morphology[10,11]. Recent experiments have shown that certain features of the cortical representation in V1 (ocular dominance) are established before the photoreceptors are functional[12]. On the other hand, these features can be altered by visual experience[13–16]. Hence, differences in the visual experience between monochromats and normal controls could cause differences in their cortical maps[17].

The specific question we asked was this: how does visual cortex in the rod monochromat develop in the large region that ordinarily receives pure cone input? This region, which had no detectable activity during rod (scotopic) vision in normal controls, was active in the brains of rod monochromats. Hence, there was an experience-dependent filling-in of the cortical activity during development. This rearrangement of the cortical representation did not occur during the transition from cone (photopic) to rod vision in normal controls. Finally, we quantified the visual representations in the brains of these rod monochromats in area V1.

Results

We measured functional magnetic resonance imaging (fMRI) responses to an expanding-ring stimulus (phase-encoded retinotopy) to determine the representation of visual field eccentricity in normal and monochromat subjects[18]. Figure 1a shows a flat representation of the left hemisphere centered on the occipital pole of a normal subject. The color overlay represents visual field eccentricity (see **Fig. 1a**, inset upper right) under photopic viewing conditions; the large foveolar representation (orange/yellow) is evident. The regular organization of topography is also evident in this view. The average time series during one cycle of the expanding ring are shown in the graphs. The time-series data were pooled from regions of interest spanning 2 cm diameter on the folded brain and centered either in the foveolar (white disk) or parafoveal (gray disk) representations. The phase of the average time series measures the visual field location that evokes the maximal response as the expanding ring passes through the visual field. Hence, the time series in the foveolar region was phase-advanced in comparison with the time series in the parafoveal region.

The response from the same cortical regions in the same subject was measured under rod viewing conditions (**Fig. 1b**). In this experiment, the mean level of illumination and the color contrast of the expanding rings were chosen so that the flickering stimulus excited only rod photoreceptors. The average time series in the foveolar representation differed greatly: while this region responded in close synchrony to the cone-initiated stimulus (**Fig. 1a**), it did not follow the rod-initiated stimulus (**Fig. 1b**). The signal in the region of interest drawn from the parafoveal visual field shared the same phase in scotopic and photopic measurement conditions.

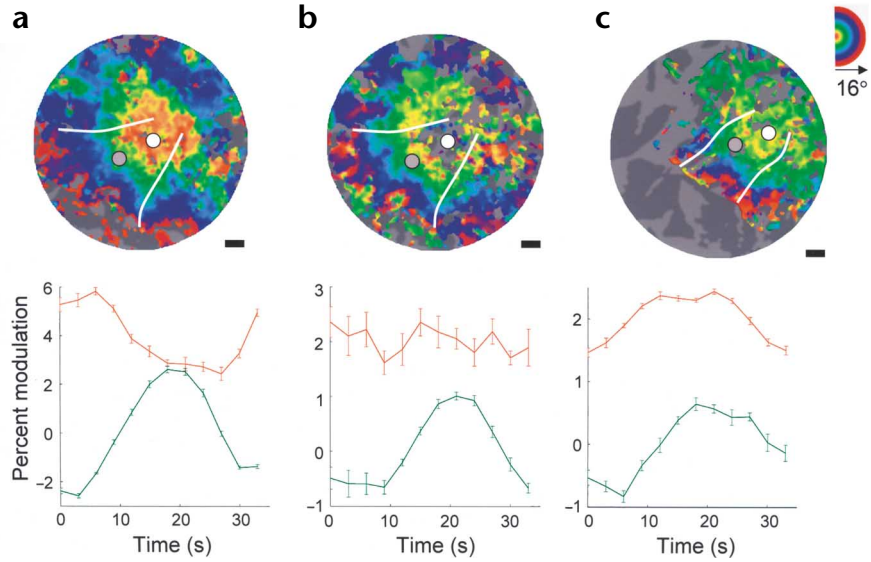

Fig. 1. Visual field eccentricity plots in three experimental conditions. The upper row shows unfolded representations of visual cortex centered on the occipital pole. The color overlay encodes the visual field eccentricity map measured using an expanding-ring stimulus. The orange/yellow overlay represents the most central regions (<2 deg), green represents the parafoveal (5–8 deg) and blue/purple represents the periphery (8–16 deg; see inset upper right of **c**). Visual field eccentricity is indicated at locations with a response correlation above 0.25. The solid white lines denote the boundary between areas V1/V2 as determined by measurements using a rotating-wedge stimulus (see Methods). The white and gray disks indicate the center of the foveolar and parafoveal regions of interest, respectively. The regions extend 2 cm in diameter (measured in the folded brain) around these points. The graphs plot the time series computed by averaging the fMRI signal from the foveolar (red line) and parafoveal (green line) regions. The error bars denote the standard error of the mean calculated from the 18 stimulus cycles (6 cycles in each of three scans). Scale bar, 1 cm. (**a**) Measurements from a normal subject (A.B.) under photopic viewing conditions. (**b**) Measurements from the same normal subject under scotopic conditions. (**c**) Measurements from a rod monochromat subject (S.H.).

We found that after dark-adaptation periods ranging from half an hour to 6 days, the rod- and cone-activated maps agreed except for the foveolar representation. To determine whether cortical reorganization could be induced in an adult observer with normal vision, subject H.B. remained under scotopic conditions for 6 consecutive days. The subject remained indoors with all windows covered while maintaining a normal daily routine, including at least 4–5 hours of computer work per day. Darkened goggles were worn while awake, and a blindfold at night, and all light sources were dimmed or filtered so that the subject was forced to use only the highly sensitized rods during this time. The subject reported a complete absence of color vision and the presence of a central scotoma under these conditions. Retinotopic mapping scans were measured numerous times, including immediately before the dark-adaptation period, to establish a baseline map in the subject, which was highly reproducible. Several retinotopic mapping scans were also measured at the end of the dark-adaptation period, and also immediately after the subject first adapted to photopic conditions (bright light, when primarily cones are active). Details were identical to those described for other scans of the normal subjects in the Methods section. No significant differences were found in either the rod-activated or cone-activated maps after the 6-day scotopic period. This argued against changes in normal, adult cortical topography due to short-term plasticity or the unmasking of inputs[19–22].

Across normal subjects, the large foveolar representation always falls in roughly the same location, slightly lateral to the occipital pole. What are the signals in this brain region of rod monochromats, who have virtually no cone inputs? In the left occipital lobe of one of the three rod monochromats there was a strong response in the region of interest that ordinarily represents foveolar signals despite the absence of cone inputs (**Fig. 1c**, white disk). The response phase coded a parafoveal representation (yellow/green) in contrast to the foveolar response phase (orange/yellow) measured in the normal photopic subject. The average time series

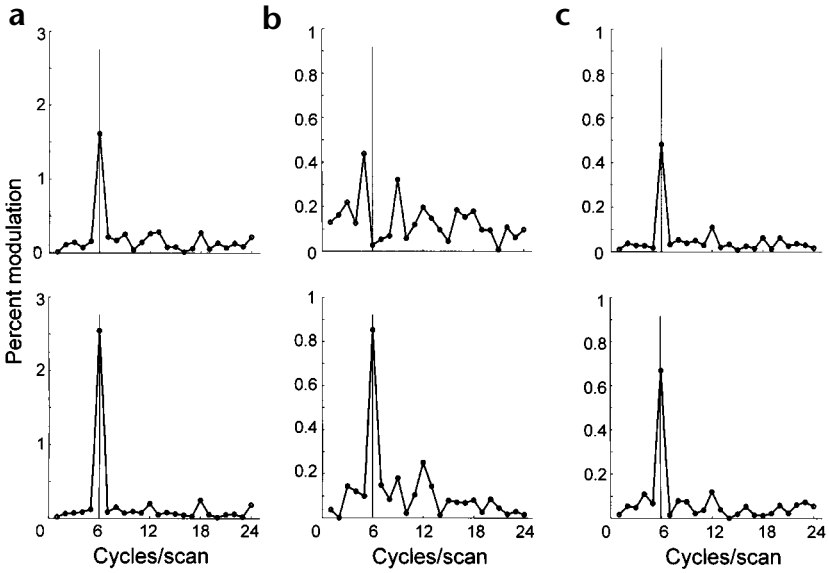

Fig. 2. Responses in foveolar and parafoveal regions in three experimental conditions. Each graph shows the amplitude in a range of temporal frequencies near the stimulus frequency (6 cycles/scan). The upper row of graphs measures the foveolar regions of interest (see white disks in **Fig. 1**) and the lower row measures the parafoveal regions (see gray disks in **Fig. 1**). (**a**) Time-series measurements from a normal subject (A.B.) under photopic conditions. (**b**) Time-series measurements from the same normal subject under scotopic conditions. (**c**) Time series measurements from a rod monochromat subject (S.H.). The gray shaded line indicates the stimulus frequency.

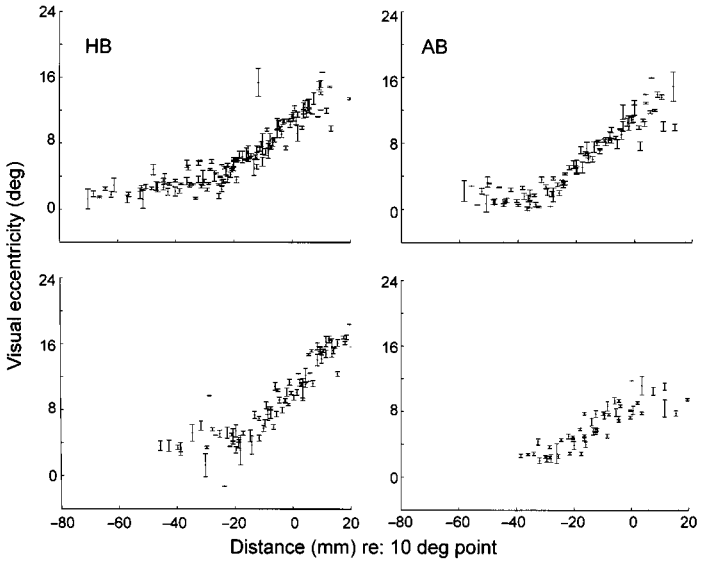

Fig. 3. Visual field eccentricity plots in V1 for two normal trichromats (H.B., A.B.). The visual field eccentricity is plotted as a function of cortical distance, where 0 mm represents a point in cortex that responds maximally to a stimulus at 10 deg eccentricity. Photopic (top panel) and scotopic (bottom panel) measurements are shown for each subject. Only points with a response correlation exceeding 0.25 were included. Data from left and right hemispheres were combined in each plot. Error bars represent ±1 s.e.m.

in the two regions of interest are compared in the bottom of Figure 1c. In both cases the response modulated in synchrony with the stimulus, as it did for the normal photopic subject. But the response phase in the region that ordinarily responds to the foveola was shifted closer to the response phase of the parafoveal representation (gray disk).

In both hemispheres of each of the three rod monochromats, we measured a powerful signal in the region of visual cortex that normally represents the foveola. Thus, in the rod monochromat brain, the cortical zone normally driven by the central cone-rich regions of the visual field had been recruited by rod-initiated inputs.

Figure 2 represents the average time series in a format that emphasizes the differences in the three measurement conditions. These graphs show the amplitude of the average time series at a range of temporal frequencies near the stimulus frequency (6 cycles/scan). Comparing the foveolar responses, there was a large reduction in signal/noise ratio as the stimulus changed from photopic to scotopic conditions (upper graphs of **Fig. 2a** and **b**), and there was no reliable scotopic response. Comparing the parafoveal representations, there was a much smaller reduction in this ratio (lower graphs of **Fig. 2a** and **b**) and a very reliable scotopic response. In contrast, there was a powerful response at the signal frequency in both foveolar and parafoveal regions within the brain of this rod monochromat (**Fig. 2c**). This stimulus-driven signal was present in the nominally foveolar representations of the two additional rod monochromats.

The spatial organization of the visual field eccentricity maps can be described quantitatively by measuring how the visual field representation varies with cortical distance. To make these measurements, we have developed automated tools for identifying the location of isoangle contours within area V1—that is, radial paths emanating from the fovea. Along each such path, visual field eccentricity was measured as a function of cortical distance (see Methods). We refer to these data as visual field eccentricity plots.

The photopic visual field eccentricity plots from the normal subjects accurately reproduced the eccentricity plots described earlier[18] (**Fig. 3**). The scotopic plots followed the same form in the periphery, but the signals became too small to measure reliably in the foveola. In these two cases, the foveolar representation spanned 2 cm of cortical distance[6].

The parafoveal representations of the rod monochromats (**Fig. 4**) covered a much larger cortical distance than the corresponding representation in normal controls measured under scotopic conditions (**Fig. 3**). Remarkably, the visual field eccentricity plot for S.H. appeared nearly like the normal photopic eccentricity plot, extending the same total distance. For D.G., the eccentricity plot also extended over roughly the same distance as the normal controls (bearing in mind that there was considerable variability in the size of V1 across normal subjects[23]). Although the data became noisy near the central fovea, the near foveal representation was approximately constant and consistent with the measurements in S.H. The data obtained from K.N. extended over the same distance, but they were somewhat less regular than the data of S.H. or D.G. The noisy points came from his right hemisphere, which produced a weaker signal than the left.

The difference between the eccentricity plots of the monochromats and normals under scotopic conditions was not described by a lateral shift of the curves; no amount of horizontal shift would bring the monochromat curves into register with the normal scotopic curves. The parafoveal signal spanned more cortical area in the monochromats than in the normal subjects, thus usurping territory normally devoted to central foveolar signals.

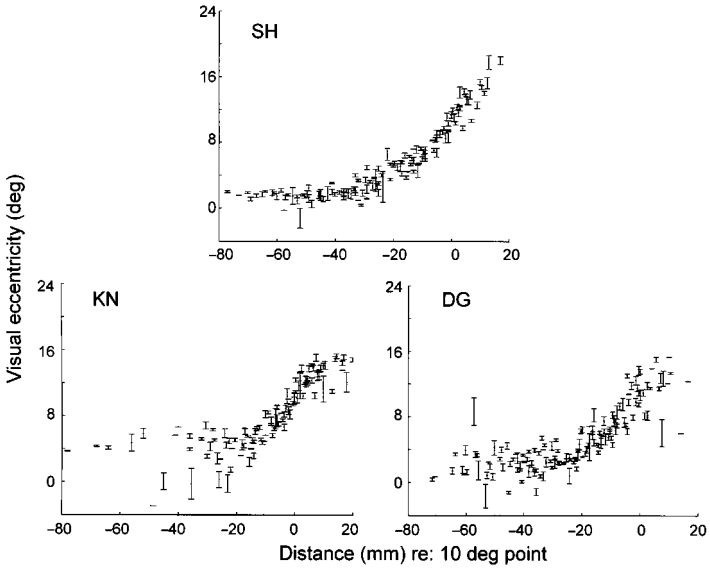

Fig. 4. Visual field eccentricity plots in V1 for three rod monochromats (S.H., D.G., K.N.). These data were measured using low-luminance conditions (7 cd/m^2). Other details are as in Figure 3.

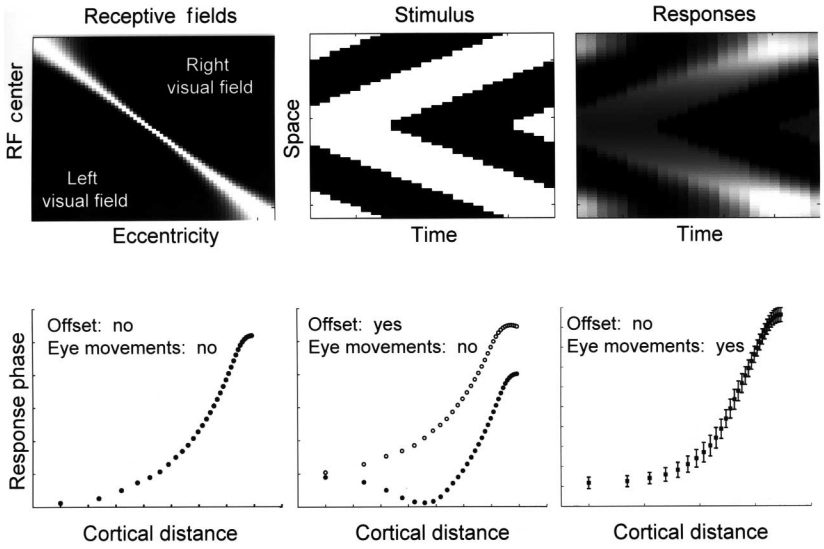

Fig. 5. Theoretical analysis and simulation of the visual field eccentricity plot. The upper left image shows the simulated one-dimensional receptive field array as an image. Each row represents the profile of a different simulated receptive field center, and the columns represent receptive fields at various eccentricities. The smallest receptive fields, in the middle columns, are in the fovea. The middle image on the top row shows the space–time diagram of the expanding square wave stimulus (1D example). White indicates the presence of the expanding-ring reversing-checkerboard, whereas black indicates a mean luminance gray background. The upper right image shows the RF responses over time. The lower panels represent the measured phases in three different conditions. See text for further explanation.

The visual field eccentricity plots comprise data from both hemispheres. Apart from the reduced signal in subject K.N. (see above), no significant differences were found between the two hemispheres. Hence, the reorganization was very similar in the two hemispheres.

Discussion

It is likely that development in the monochromats proceeds normally up until birth, when photoreceptor stimulation is ultimately required to play a role in further development[17,24]. Therefore, the observed changes were a direct result of visual system plasticity in response to their altered visual experience. These changes could be mediated by a variety of mechanisms, including reorganization of neural connectivity and changes in the efficacy of established connections.

Measurements in monochromats require some special considerations of their unique visual characteristics. They often exhibit behavioral symptoms indicative of compromised cone function and a lack of central foveal vision, including slightly eccentric fixation and intensity-dependent optical nystagmus[11,25,26]. These factors can be ruled out as possible explanations of our results.

First, consider that the distribution of responses across cortex reflect the input of direct axonal connections from the retina via the lateral geniculate nucleus. No amount of fixational shift or eye movement can influence the arrangement of these connections. The presence of a response in the normally rod-free foveolar representation, therefore, must result from changes in the wiring somewhere along the input pathways to visual cortex. Thus, the main conclusion of this paper—that this rod-free foveolar representation in normal cortex was powerfully activated in rod monochromats—was clearly demonstrated.

While eccentric fixation or nystagmus cannot cause the hardwired, rod input-free zone to respond, such effects might influence the quantitative measurements of visual field eccentricity plots. Eccentric fixation was measured in each of the monochromat subjects outside the scanner and ranged between 0.5 and 2 deg. Fixation in the rod monochromats was shifted either toward the left (K.N., S.H.) or right (D.G.) visual field.

We simulated the effects of eccentric fixation and nystagmus for a simple one-dimensional model (**Fig. 5**). The top left panel represents a set of neuronal receptive field functions that vary in size from fovea to periphery. The middle image represents an expanding square wave. The image on the right shows the time series of each simulated neuron. The graph on the lower left shows the expected eccentricity map for a subject with these receptive fields, perfect fixation and no nystagmus. This curve is very close to the measurements we obtained in normal controls,

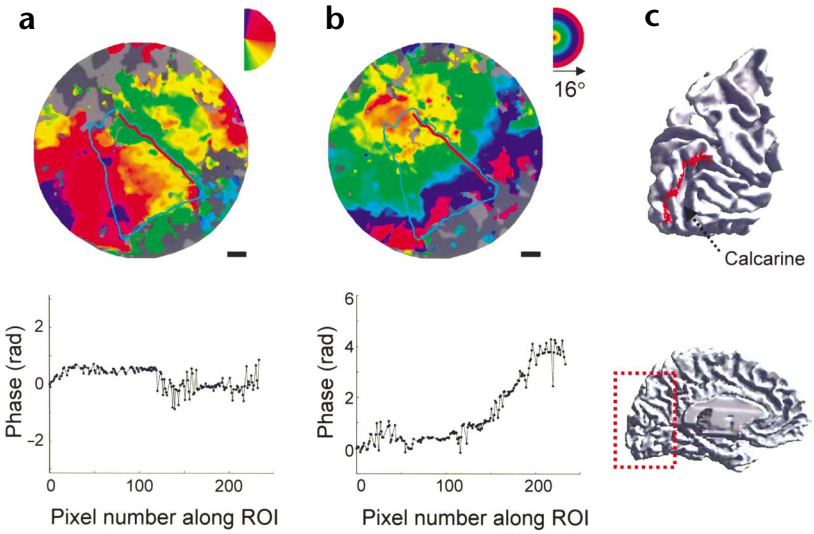

Fig. 6. Visual field eccentricity measurement methods. (**a**) Phase-encoded retinotopic response to the rotating-wedge stimulus on a flattened representation of occipital cortex. Color encodes visual angle (see inset in upper right of **a**). The cyan outline is the boundary of V1 determined by an automated tool. The red line denotes a region of interest (ROI) along an isoangle path within V1; such paths were projected back into the folded brain where we calculated all cortical distances. (**b**) The same V1 boundary and ROI overlaid on a phase-encoded retinotopic response to the expanding ring stimulus. Color now encodes visual eccentricity (see inset in upper right of **b**). The plot measures the change in eccentricity along the ROI. (**c**) The isoangle ROI mapped onto a 3D rendering of this brain. Its position is near the upper lip of the calcarine sulcus.

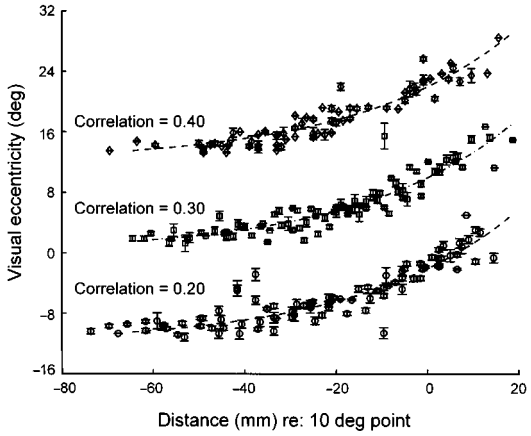

Fig. 7. Visual field eccentricity plots are independent of correlation threshold. The visual field eccentricity plot, measured at three different correlation levels, is shown for one normal subject (H.B.) in an expanding-ring experiment. The points chosen at different correlation levels have been displaced for comparison. Points with at least 0.20 correlation are shifted down (circles); points with at least 0.30 correlation are not shifted (squares); points with at least 0.40 correlation are shifted up (diamonds). Error bars indicate ±1 s.e.m.

including the rounding at the upper right. In the simulation, this rounding was caused by signals from neurons with large receptive fields centered just outside the stimulus region.

The lower middle graph shows the effect of a systematic horizontal shift in fixation. This produced an asymmetric response in the cortical maps in the two occipital lobes. The simulated curves show the effects in the event that a subject fixated 1.6 deg eccentrically. Such deviations could be detected by our measurements, but they were not present. As we described above, the data from the two hemispheres were well matched in all of the rod monochromats. Hence, the agreement of cortical maps in the two hemispheres and the lack of any representation of the center of the stimulus suggested that the monochromats were largely fixating such that the stimulus was centered on their inactive fovea, rather than eccentrically.

Fixation stability was assessed in each potential monochromat subject and formed a basis for selection (see Methods). At the low light levels used in our experiments, nystagmus was greatly reduced or nonexistent. In general, fixation instability would tend to locally smear the retinotopic maps, reducing activity, rather than producing activity where none is present. In fact, we observed precisely such diminished foveal responses in control measurements made on a subject with significant nystagmus. In separate experiments, we performed retinotopic mapping on a subject with congenital nystagmus of 3 deg peak-to-peak amplitude. The visual field eccentricity plot in this subject differed from normal only in the degree of noise in the data. Unlike the measurements in the subject with nystagmus, the monochromats showed a clear, robust retinotopic map on the medial surface. The differences between normal and monochromat retinotopic maps were unlike the differences between maps of normals and subjects with nystagmus, presumably because we selected the viewing conditions to minimize nystagmus in monochromats.

Additionally, the lower right graph in Figure 5 shows the simulated results of random eye movements by the rod monochromats. The error bars show the effects of simulating eye movements drawn from a Gaussian distribution (mean deviation zero, s.d. 1 deg). This only increased variance. Hence, our methods were robust with respect to moderate fixation instability for both normals and rod monochromats.

By comparing retinotopic representations in normal subjects with those in congenital rod monochromats, we have observed for the first time how abnormal retinal input alters the development of retinotopic maps in the human brain. The reorganization spanned roughly 4 cm^2 of cortex, far greater than can be easily observed with single-unit methods. While it is possible that changes also occurred at earlier stages such as the lateral geniculate nucleus or even the retina, there is little doubt that experience-dependent cortical remapping occurred. The molecular alterations in the genes encoding the cone photoreceptors have profound consequences for visual experience. The abnormal visual experience, in turn, changes cortical organization. Our findings illustrate the close coupling among genetics, experience and brain development.

Methods

Subjects. All subjects provided informed consent to participate in the project.

Normal: H.B. (female, age 35) and A.B. (female, age 28) both have normal, trichromatic color vision. All experiments were done in compliance with the relevant laws and institutional guidelines and were approved by the Stanford human subjects committee.

Rod monochromats: K.N. (male, age 56) has been studied extensively. He consistently demonstrates a lack of any cone function[26]. Molecular genetic analysis reveals homologous missense mutations in a gene (*CNGA3*) on chromosome 2 that encodes the α-subunit of the cGMP-gated cation channel in the cone photoreceptors, rendering the cones unexcitable[7]. Fixation is less precise than normal, with deviations as great as ±2 deg, as measured with a scleral search coil[25]. D.G. and S.H. (males, age 27 and 29, respectively) have both been clinically diagnosed as rod monochromats[27,28], although molecular genetic analysis has not established their origin. Some residual cone function can be demonstrated in both D.G. and S.H., but only under conditions of extreme light adaptation not used during the fMRI scans. Preferred fixation position was mapped relative to the blind spot (optic nerve head), and fixation stability was assessed using a standard ophthalmoscope. In their preferred eyes, which were used in these experiments, fixation was deviated horizontally by 1.5–2 deg (S.H.) and 1 deg (D.G.).

Stimuli. Retinotopic mapping methods were similar to those published previously[18,29]. Retinal eccentricity was mapped using a contrast-reversing (4 Hz) checkerboard presented within an expanding annular ring (maximum diameter 32 deg). The ring slowly expanded from the central to peripheral field, starting again in the center as the 16 deg radius was passed. A single expansion cycle lasted 36 s, and was repeated for 7 cycles. All data shown are from the average of three such scans.

Each visual field location alternated between a reversing check pattern for 18 s and a uniform gray field for 18 s during each cycle, and the phase of the alternation coded visual field position. The check pattern fundamental spatial frequency was close to 0.25 cycles/deg, although it varied slightly from center to periphery because of the dartboard configuration of the pattern. In all stimulus conditions, the first cycle (36 s) was excluded from analysis to remove transient artifacts at stimulus onset. A large 'X' (32 × 32 deg) centered over the stimulus was used as a fixation guide.

Silent substitution methods were used to stimulate selectively the different receptor classes in the normal subjects[30]. For the normal subjects, the mean luminance under cone conditions was 70 candela (cd) per m^2. To preferentially activate rods in the normals, the mean field luminance was reduced to 0.07 cd/m^2 using neutral density filters, and modulation of the check pattern was metameric to modulation of a 500 nm light. The rod monochromats viewed black/white check patterns through 1 log unit neutral density filters (mean luminance, 7 cd/m^2), as silent substitution methods were unnecessary. In cases where fixation in one eye was more stable than the other, data were collected monocularly (D.G., right eye; S.H., left eye). No significant differences were found between monocular or binocular retinotopic maps measured in K.N. and in normals.

Scanning procedure. Monochromats and one normal control (H.B.) were tested in a supine position in a 1.5-Tesla (T) GE Signa scanner (Milwaukee, Wisconsin). A second normal control (A.B.) was tested in a 3-T GE Signa scanner. The stimuli were presented using a flat-panel LCD monitor (NEC 2000, Santa Clara, California) and publicly provided software[31]. Subjects viewed the display through a pair of binoculars with mirrors mounted above the head, which could be adjusted to correct for individual alignment and refractive error. The head was immobilized using a bite bar or padding. Subjects maintained fixation on a mark centered on the stimulus throughout each scan. Functional magnetic resonance images (T2*-weighted blood-oxygenation level-dependent responses[32]) were collected in planes perpendicular to the calcarine sulcus through the occipital lobes using a two-dimensional spiral sequence[33] (1.5 T: 8 planes, 2 spiral interleaves; TR, 1,500 ms; TE, 40 ms; flip angle, 90°; voxel resolution, $1.9 \times 1.9 \times 4$ mm; 3 T: 23 planes, 2 spiral interleaves; TR, 1,500 ms; TE, 30 ms; flip angle, 70°; voxel resolution, $1.7 \times 1.7 \times 3$ mm). A high-resolution anatomical (T1-weighted) MRI volume scan of the entire head was also run on each subject (voxel size, $0.9 \times 0.9 \times 1.2$ mm).

Data analysis and visualization. To create time-series plots, the fMRI time series at each voxel were recorded and converted from arbitrary units to a scale that measures percentage change with respect to the mean voxel level. Linear trends were removed, but no further processing was performed. For each experimental condition, we computed the average fMRI time series from three scans. To measure the phase and amplitude of the fMRI response at each voxel, we transformed this time series into a Fourier amplitude spectrum. We then measured the phase and amplitude of the time series at the stimulus alternation rate of 1/36 Hz. The response phase of each voxel encodes the eccentricity (phase-encoded retinotopy). Gray matter was segmented from the high-resolution anatomical scan for each subject, rendered in three dimensions close to the white matter boundary and unfolded using publicly available software[34,35]. Functional activity from all cortical layers was projected onto the unfolded representation to the closest location on the white matter boundary.

Figure 6 illustrates several important aspects of our methods. First, the positions of primary visual cortex (V1) and other visual areas were determined in each subject from the visual field representation on the unfolded surface[29]. The areas were identified using an automatic tool that minimized the error between the expected visual map (atlas) and the observed data (V.M. Koch *et al.*, *Soc. Neurosci. Abstr.*, Vol. 27, Program No. 620.14, 2001). In this tool, the atlas is coarsely aligned with the data and then elastically deformed. The elastic deformation is chosen to fit the measured data by minimizing an energy function. Figure 6a and b show examples of phase-encoded retinotopy data on a flattened representation of the left occipital lobe. One region of interest indicates the perimeter of the V1 region that was found by the elastic deformation of a V1 atlas. The second region of interest represents an isoangle contour taken from the fitted atlas but mapped onto the folded cortical surface.

The graphs in Figure 6a and b show the measured response phases along the isoangle contour. The atlas fit the data well; the angular representation along a constant isoangle path in the atlas follows a constant phase to a rotating-wedge stimulus (**Fig. 6a**). Along this path the eccentricity map increases as one expects (**Fig. 6b**). Figure 6c contains both a three-dimensional rendering of the occipital lobe that depicts the location of the flattened representation, and then an expanded view of this occipital lobe indicating the region of interest near the upper lip of the calcarine sulcus. The measurements described in this paper were all obtained by first finding V1 using this automated tool, then selecting several isoangle paths and transforming these paths onto the folded brain and, finally, measuring distances and response phases along the convoluted cortical surface. The data from 8–20 isoangle regions of interest were pooled into a single eccentricity plot such as those plotted in Figures 3 and 4.

Finally, we note that there are often differences between subjects in the reliability of the measured signal. Indeed, over the years, as instruments and methods have improved, we now obtain data that are far superior to our early measurements. This improvement in signal:noise did not change the eccentricity plots we measured. The eccentricity plots were measured at three different correlation levels, with the three data sets and curves displaced vertically for clarity (**Fig. 7**). The agreement between the data and the curves showed that the visual field eccentricity plot was invariant across this range of correlation thresholds. Indeed, all three were fitted by the curve $\text{deg} = \exp(s \times \text{dist} + 2.3)$, where deg is the visual eccentricity and dist is the distance along cortex in millimeters measured from a reference position in cortex that responds maximally to a stimulus at 10 deg eccentricity. The parameter s is a scale factor that differs among people and ranges from 0.025 to 0.035.

The earliest data collected in this study had a signal:noise ratio comparable to the curve marked at a correlation level of 0.20. Currently, we typically restrict voxels to a correlation level of 0.30, as shown in the middle curve. Even if we restrict to a higher criterion (0.40, top curve), the shape of the eccentricity map is unchanged. Hence, the absolute signal level in different subjects should not influence our conclusions.

Acknowledgements

This research was supported by fellowships and grants from the National Institutes of Health (EY30164), National Eye Institute (NEI), North Atlantic Treaty Organization, the Wellcome Trust and the McKnight Foundation. We are grateful to G. Haegerstrom-Portnoy and M. Schneck for referring and providing clinical data on D.G. and S.H. We also thank R. Dougherty, G. Haegerstrom-Portnoy, D. Heeger, S. Heinen, R. Hoffman, V. Koch, W. Newsome, W. Press, M. Schneck and A. Wade.

Competing interests statement

The authors declare that they have no competing financial interests.

RECEIVED 14 JANUARY; ACCEPTED 28 JANUARY 2002

1. Østerberg, G. A. Topography of the layer of rods and cones in the human retina. *Acta Ophthamol.* **6**, 1–103 (1935).
2. Polyak, S. L. *The Retina* (Univ. of Chicago Press, Chicago, IL, 1941).
3. Ahnelt, P. K., Kolb, H. & Pflug, R. Identification of a subtype of cone photoreceptor, likely to be blue sensitive, in the human retina. *J. Comp. Neurol.* **255**, 18–34 (1987).
4. Curcio, C. A., Sloan, K. R., Kalina, R. E. & Hendrickson, A. E. Human photoreceptor topography. *J. Comp. Neurol.* **292**, 497–523 (1990).
5. Horton, J. C. & Hoyt, W. F. The representation of the visual field in human striate cortex. A revision of the classic Holmes map. *Arch. Ophthalmol.* **109**, 816–824 (1991).
6. Hadjikhani, N. & Tootell, R. B. Projection of rods and cones within human visual cortex. *Hum. Brain Mapp.* **9**, 55–63 (2000).
7. Kohl, S. *et al.* Total color-blindness is caused by mutations in the gene encoding the α-subunit of the cone photoreceptor cGMP-gated cation channel. *Nat. Genet.* **19**, 257–259 (1998).
8. Kohl, S. *et al.* Mutations in the *CNGB3* gene encoding the β-subunit of the cone photoreceptor cGMP-gated channel are responsible for achromatopsia (*ACHM3*) linked to chromosome 8q21. *Hum. Mol. Genet.* **9**, 2107–2116 (2000).
9. Sharpe, L. T., Stockman, A., Jagle, H. & Nathans, J. in *Color Vision: From Genes to Perception* (eds Gegenfurtner, K. & Sharpe, L. T.) 3–52 (Cambridge Univ. Press, Cambridge, 1999).
10. Glickstein, M. & Heath, G. G. Receptors in the monochromat eye. *Vision Res.* **15**, 633–636 (1975).
11. Sharpe, L. T. & Nordby, K. in *Night Vision: Basic, Clinical and Applied Aspects* (eds Hess, R. F., Sharpe, L.T. & Nordby, K.) 335–389 (Cambridge Univ. Press, Cambridge, 1990).
12. Weliky, M. & Katz, L. C. Correlational structure of spontaneous neuronal activity in the developing lateral geniculate nucleus *in vivo*. *Science* **285**, 599–604 (1999).
13. White, L. E., Coppola, D. M. & Fitzpatrick, D. The contribution of sensory experience to the maturation of orientation selectivity in ferret visual cortex. *Nature* **411**, 1049–1052 (2001).
14. Gilbert, C. D. & Wiesel, T. N. Receptive field dynamics in adult primary visual cortex. *Nature* **365**, 150–152 (1992).
15. Kaas, J. H. Plasticity of sensory and motor maps in adult mammals. *Annu. Rev. Neurosci.* **14**, 137–167 (1991).
16. Heinen, S. J. & Skavenski, A. A. Recovery of visual responses in foveal V1 neurons following bilateral foveal lesions in adult monkey. *Exp. Brain Res.* **83**, 670–674 (1991).
17. Crair, M. C., Gillespie, D. C. & Stryker, M. P. The role of visual experience in the development of columns in cat visual cortex. *Science* **279**, 566–570 (1998).
18. Engel, S. A., Glover, G. H. & Wandell, B. A. Retinotopic organization in human visual cortex and the spatial precision of functional MRI. *Cereb. Cortex* **7**, 181–192 (1997).
19. Kapadia, M. K., Westheimer, G. & Gilbert, C. D. Dynamics of spatial

summation in primary visual cortex of alert monkeys. *Proc. Natl. Acad. Sci. USA* **96**, 12073–12078 (1999).
20. Pettet, M. W. & Gilbert, C. D. Dynamic changes in receptive-field size in cat primary visual cortex. *Proc. Natl. Acad. Sci. USA* **89**, 8366–8370 (1992).
21. Das, A. & Gilbert, C. D. Topography of contextual modulations mediated by short-range interactions in primary visual cortex. *Nature* **399**, 655–661 (1999).
22. Kapadia, M., Gilbert, C. & Westheimer, G. A quantitative measure for short-term cortical plasticity in human vision. *J. Neurosci.* **14**, 451–457 (1994).
23. Andrews, T. J., Halpern, S. D. & Purves, D. Correlated size variations in human visual cortex, lateral geniculate nucleus, and optic tract. *J. Neurosci.* **17**, 2859–2868 (1997).
24. Rodieck, R. W. Visual pathways. *Annu. Rev. Neurosci.* **2**, 193–225 (1979).
25. Sharpe, L. T., Collewijn, H. & Nordby, K. Fixation, pursuit and optokinetic nystagmus in a complete achromat. *Clin. Vis. Sci.* **1**, 39–49 (1986).
26. Sharpe, L. T. & Nordby, K. in *Night Vision: Basic, Clinical and Applied Aspects* (eds Hess, R. F., Sharpe, L.T. & Nordby, K.) 253–289 (Cambridge Univ. Press, Cambridge, 1990).
27. Haegerstrom-Portnoy, G., Schneck, M. E., Verdon, W. A. & Hewlett, S. E. Clinical vision characteristics of the congenital achromatopsias. I. Visual acuity, refractive error, and binocular status. *Optom. Vis. Sci.* **73**, 446–456 (1996).
28. Haegerstrom-Portnoy, G., Schneck, M. E., Verdon, W. A. & Hewlett, S.E. Clinical vision characteristics of the congenital achromatopsias. II. Color vision. *Optom. Vis. Sci.* **73**, 457–465 (1996).
29. Wandell, B. A. Computational imaging of human visual cortex. *Annu. Rev. Neurosci.* **22**, 145–173 (1999).
30. Wandell, B. A. *Foundations of Vision* (Sinauer Press, Sunderland, MA, 1995).
31. Brainard, D. H. The psychophysics toolbox. *Spat. Vis.* **10**, 433–436 (1997).
32. Meyer, C. H., Hsu, B. S., Nishimura, D. G. & Macovski, A. Fast spiral coronary artery imaging. *Mag. Res. Med.* **28**, 202–213 (1992).
33. Ogawa, S. *et al.* Intrinsic signal changes accompanying sensory stimulation: functional brain mapping with magnetic resonance imaging. *Proc. Natl. Acad. Sci. USA* **89**, 5951–5955 (1992).
34. Teo, P. C., Sapiro, G. & Wandell, B. A. Creating connected representations of cortical gray matter for functional MRI visualization. *IEEE Trans. Med. Imaging* **16**, 852–863 (1997).
35. Wandell, B. A., Chial, S. & Backus, B. Visualization and measurement of the cortical surface. *J. Cogn. Neurosci.***12**, 739–752 (2000).